Corosolic Acid Inhibits Tumor Growth without Compromising ALPPS-induced Liver Regeneration in Rats

Jinwei zhao
second hospital of jilin university
xueyue luo
Jilin University
weiyi zhao
Yanbian University
hong zhou
Jilin University
hongyue xu
second hospital of Jilin university
xuefei wang
Jilin university
wenjing luan
Jilin University
yanan an
Jilin University
chao wang
Jilin University
Lu Yu (yu_lu@jlu.edu.cn)
jilin university

Research

Keywords: ALPPS, liver regeneration, tumor growth, corosolic acid, macrophage polarization

Posted Date: September 3rd, 2020

DOI: https://doi.org/10.21203/rs.3.rs-64913/v1

Abstract

Backgroud

The associating liver partition and portal vein ligation (ALPPS) technique is a promising strategy for unresectable tumors without sufficient future liver remnants (FLRs). Criticism has focused on its stimulation of tumor growth. This study explores the effect of corosolic acid (CA) on inhibiting tumor growth without compromising ALPPS-induced liver regeneration and investigates its possible mechanism.

Methods

The ALPPS procedure was performed in Sprague-Dawley rats with orthotopic liver cancer. Blood, tumor and FLR samples in different group were collected.

Results

The tumor weight in the implantation/ALPPS/CA group was lower than that in the implantation/ALPPS group ($p < 0.05$). On postoperative day 15, the hepatic regeneration rate and the expression of Ki67+ hepatocytes in the FLRs increased significantly in the group that underwent ALPPS. The number of CD86+ macrophages increased in the FLRs and tumors of the groups that underwent the ALPPS procedure. Additionally, the number of CD206+ macrophages was higher than the number of CD86+ macrophages in the tumors of the implantation group and the implantation/ALPPS group ($p < 0.01$, respectively); however, the opposite results were observed in the CA groups. The administration of CA downregulated the expression of TGF-β, CD31 and PD-1, whereas it increased the number of CD8+ lymphocytes in tumors.

Conclusions

CA inhibits tumor growth without compromising ALPPS-induced liver regeneration. This result may be attributed to the CA-induced downregulation of PD-1 and TGF-β expression and the increased CD8+ lymphocyte infiltration in tumor tissue, associated with the suppression of M2 macrophage polarization.

Full Text

This preprint is available for download as a PDF.

Figures

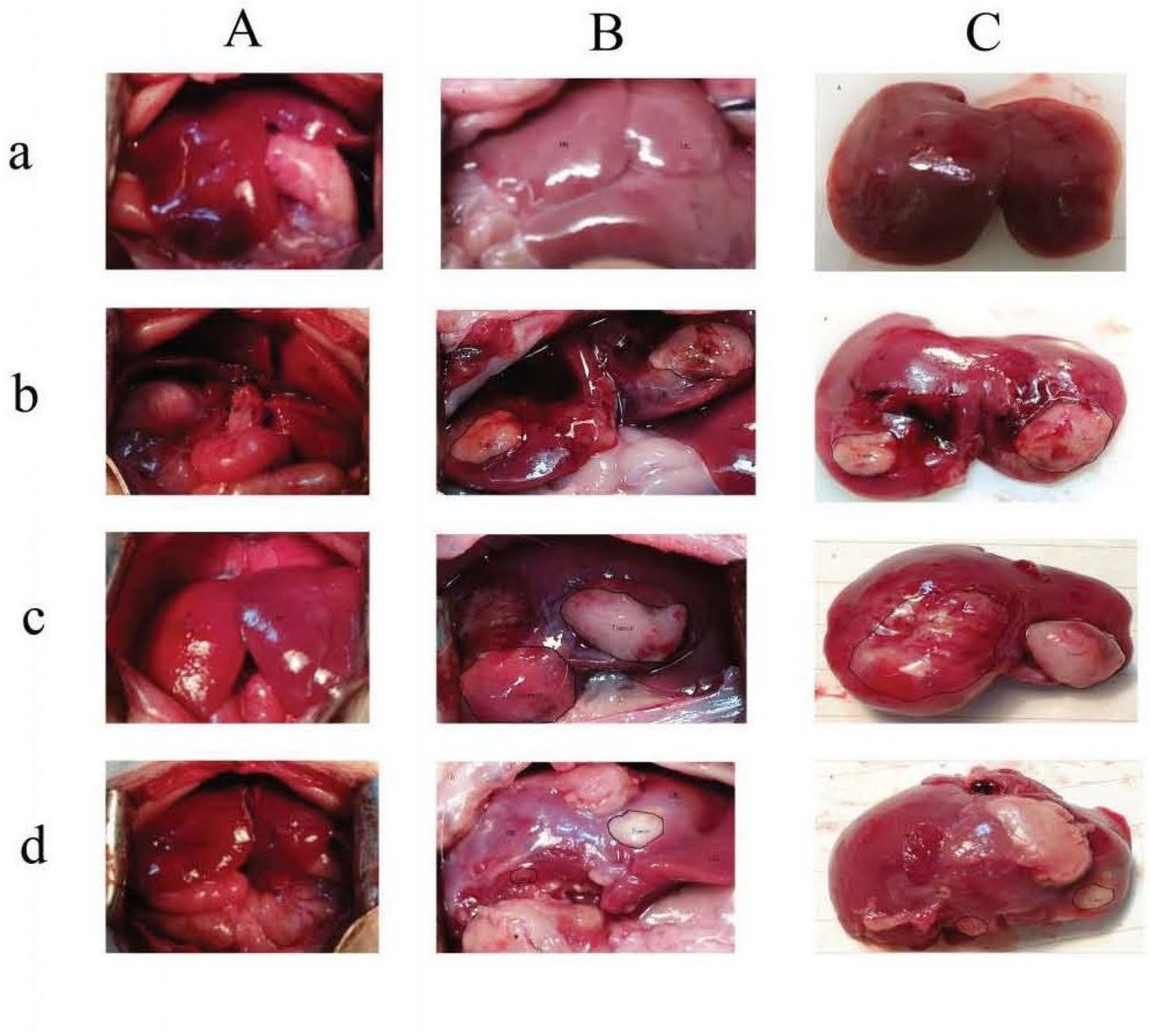

Figure 1

Illustrations of surgical operation. A, The ALPPS procedure in rats with orthotopic liver cancer. a: Exposure of the liver after laparotomy; b: Ligation of portal vein branches. The silk knots represent the ligated portal vein (PV); 1 presents the PV of the right lobe (RL); 2 presents the hepatic pedicle of the caudate lobe (CL) and resected CL; 3 presents the PV of the left median lobe (LML) and left lateral lobe (LLL); c: An ischemic line emerged slightly to the right of the falciform ligament; d: The median lobe (ML) was split in situ along the ischemic line and implant tumor tissue. B, Exposure of the liver at POD15: a: Group 1, normal liver; b: Group 2, the tumor observed within the LML and RML; c: Group 3, FLR (RML) regeneration, enlarged tumor observed within the LML and RML. d: Group 4, FLR (RML) regeneration, reduced tumor observed within the LML and RML. C, The resected ML. a, Group 1: sham group; b, Group 2: implantation without ALPPS group; c, Group 3: implantation/ALPPS group; d, Group4: implantation/ALPPS/CA group.

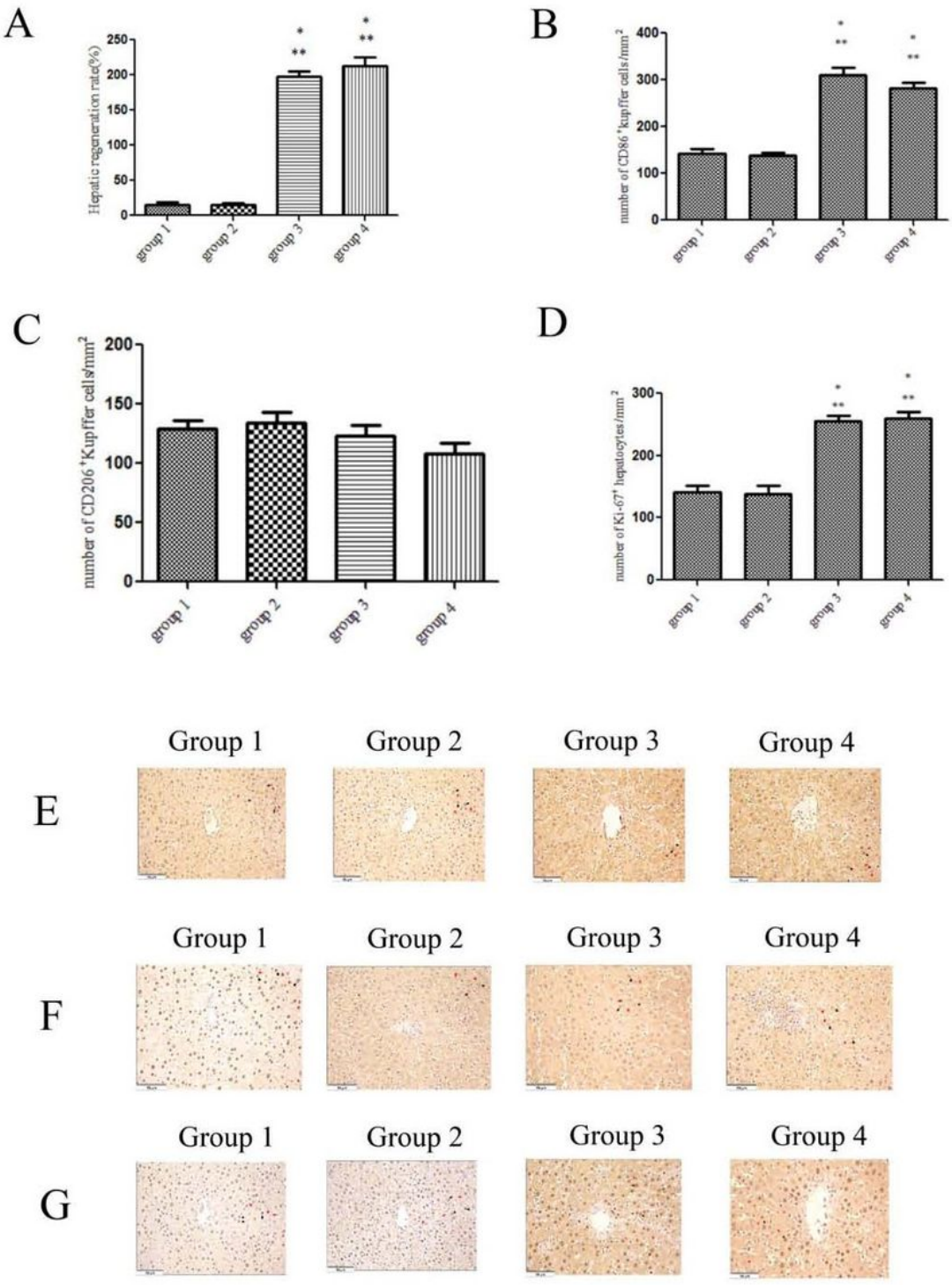

Figure 2

ALPPS-induced liver regeneration (HRR) is closely related to CD86+ Kupffer cells. A, HRR; B, The number of CD86-positive Kupffer cells per square millimeter; C, The number of CD206-positive Kupffer cells per square millimeter; D, The number of Ki-67-positive hepatocytes per square millimeter; E, Immunohistochemical staining for CD86 in regenerating lobes in each group; F, Immunohistochemical staining for CD206 in regenerating lobes in each group; G, Immunohistochemical staining for Ki-67 in

regenerating lobes in each group; H, Immunohistochemical staining negative control image in normal liver; Scale bars, 50μm. *, p < 0.01 group 1 compared with group 3 or group 4; **, p < 0.01 group 2 compared with group 3 or group 4. Cells with nuclear deposition of violet pigment were positive(black arrow), nuclear deposition of blue pigment were negative(red arrow) (original magnification 200 ×). Values are means ± SD. Group 1: sham group; Group 2: implantation without ALPPS group; Group 3: implantation/ALPPS group; Group4: implantation/ALPPS/CA group.

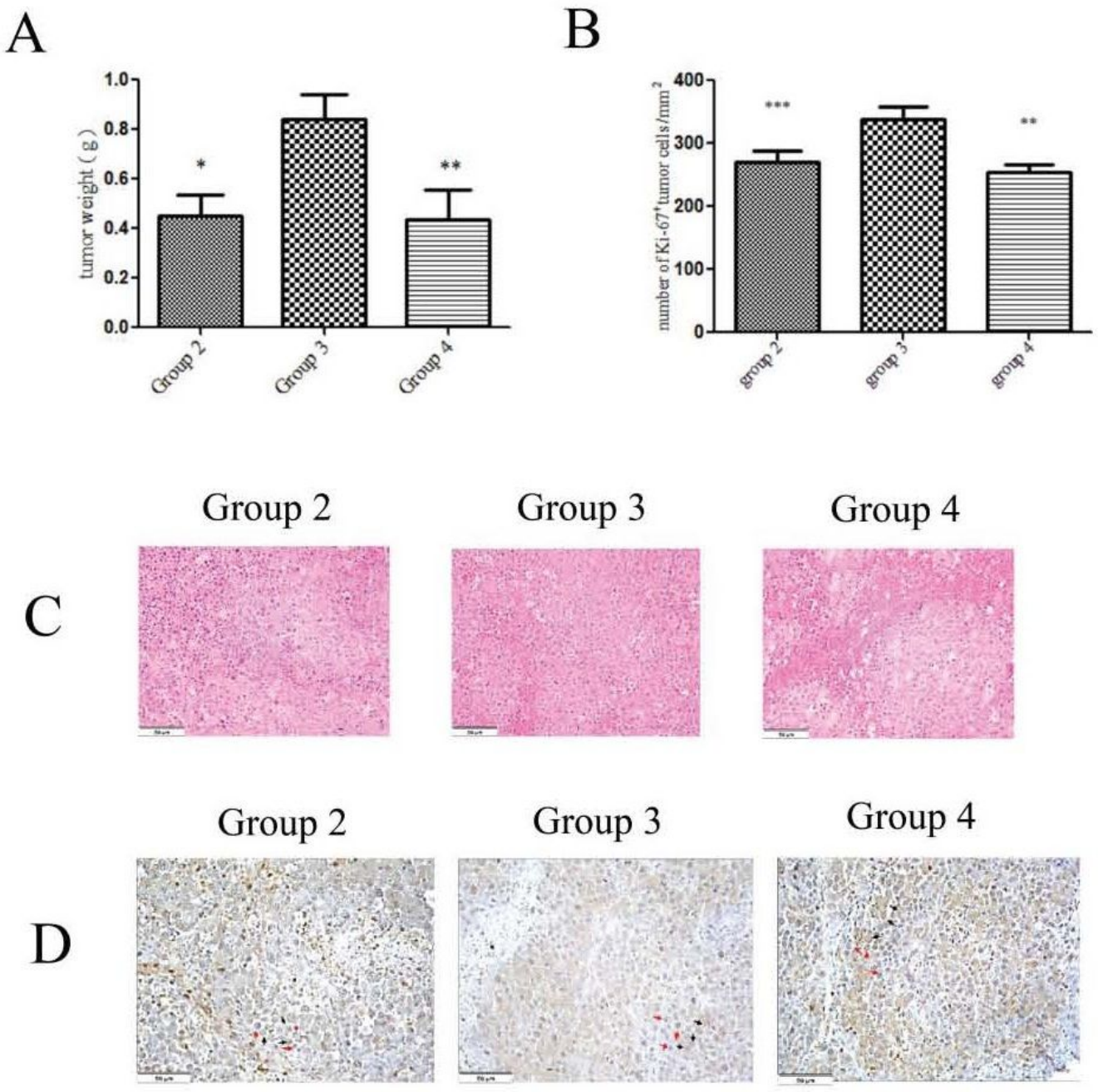

Figure 3

CA inhibits tumor growth without compromising ALPPS-induced liver regeneration. A, The tumor inhibition rate under CA treatment; B, The number of Ki-67-positive tumor cells per square millimeter; C, HE staining for tumor cells in regenerating lobes in each group; D, Immunohistochemical staining for Ki-67 in tumor tissue in regenerating lobes in each group. Scale bars, 50μm. *, $p < 0.01$ group 2 compared with group 3; **, $p < 0.01$ group 3 compared with group 4; ***, $p < 0.05$ group 2 compared with group 3. HE staining with nuclear deposition of violet blue was positive, and immunohistochemical staining for Ki-67 cells with nuclear deposition of violet pigment were positive(black arrow), nuclear deposition of blue pigment were negative(red arrow) (original magnification 200 ×). Values are means ± SD. Group 1: sham group; Group 2: implantation without ALPPS group; Group 3: implantation/ALPPS group; Group4 implantation/ALPPS/CA group.

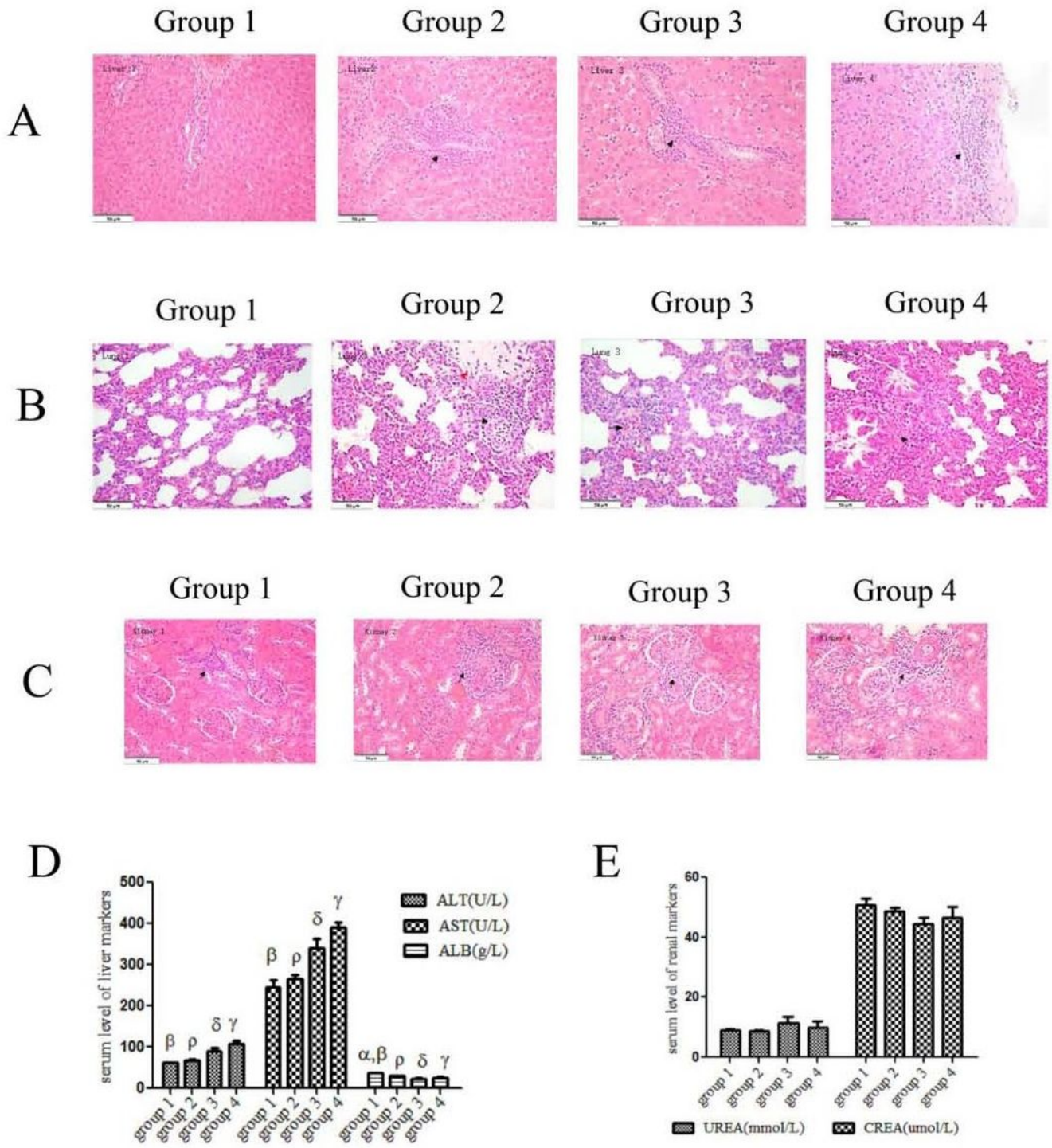

Figure 4

Organ damage and change in liver-renal function after ALPPS. A, HE staining for liver in regenerating lobes in each group. No histopathological findings were observed in group 1; inflammatory cell infiltration in the portal area and thickness of the Glisson capsule were observed in the other 3 groups (black arrow). B, HE staining of lung in each group. Inflammatory cell infiltration was observed in group 1 (black arrow); pulmonary interstitial edema, inflammatory cell infiltration (black arrow) and wideness of the alveolar

septum (red arrow) were observed in group 2; pulmonary interstitial edema and inflammatory cell infiltration were observed in the other 2 groups (black arrow). C, HE staining of kidney in each group. Inflammatory cell infiltration of small arteries and para-arterioles in the renal cortex was observed in each group (black arrow). D, Liver function. E, Renal function. Scale bars, 50μm. α, p < 0.01 group 1 vs. group 2; β, p < 0.01 group 1 vs. group 3; , p < 0.01 group 1 vs. group 4; δ, p < 0.01 group 2 vs. group 3; ρ, p < 0.01 group 2 vs. group 4. Values are means ± SD. Group 1: sham group; Group 2: implantation without ALPPS group; Group 3: implantation/ALPPS group; Group4: implantation/ALPPS/CA group.

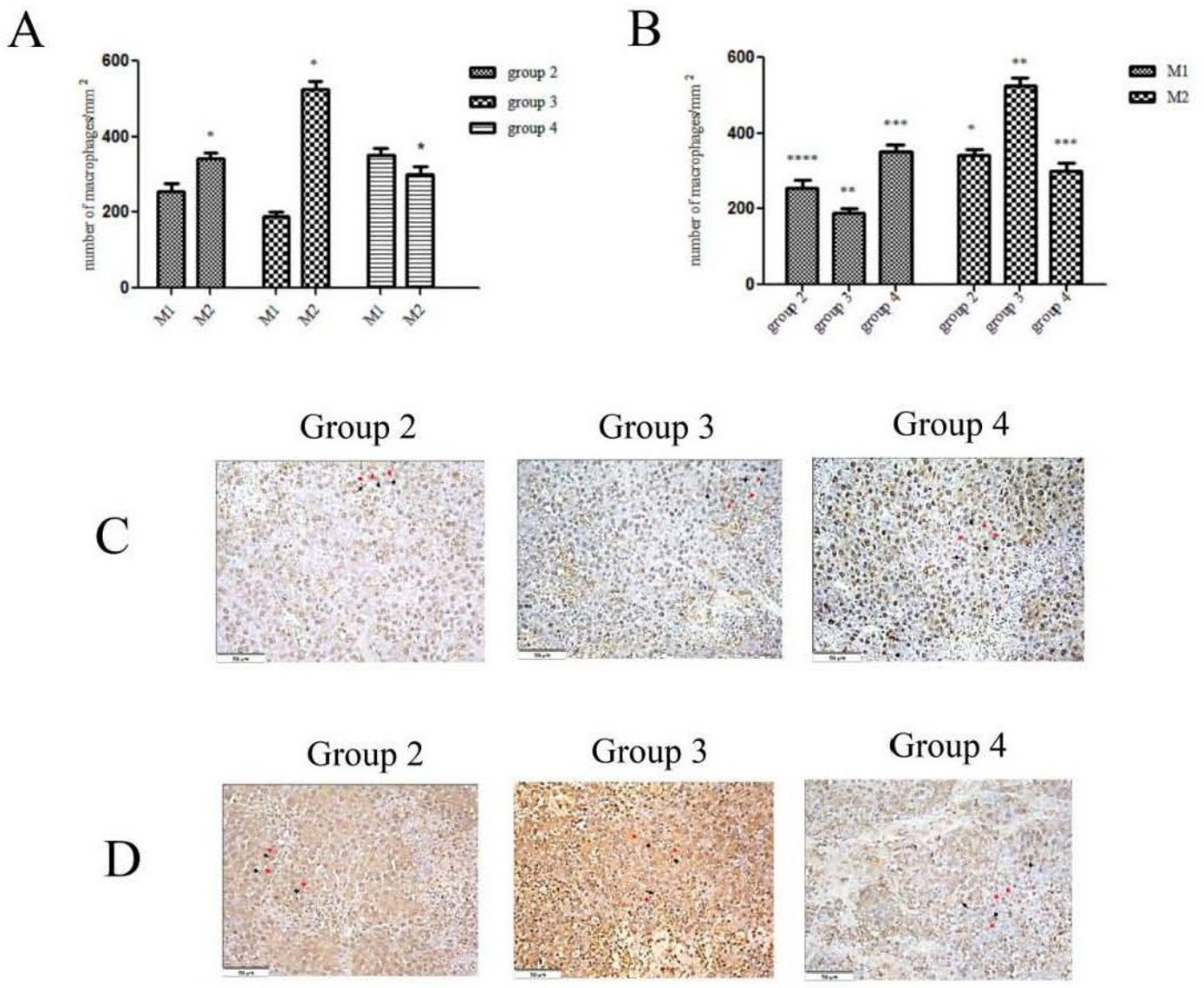

Figure 5

Administration of CA increases M1 and decreases M2 macrophages in tumors. A, The proportion of M1 macrophages and M2 macrophages per square millimeter in each group with implanted tumors; B, The number of M1 macrophages and M2 macrophages per square millimeter in each group with implanted tumors; C, Immunohistochemical staining for CD86+ macrophages in tumor tissue in each group with

implanted tumors; D, Immunohistochemical staining for CD206+ macrophages in tumor tissue in each group with implanted tumors; E, Immunohistochemical staining negative control image in tumors. Scale bars, 50μm. *, p < 0.01 M1 vs. M2; group 2 vs. group 3; **, p < 0.01 group 3 vs. group 4; ***, p < 0.01 group 2 vs. group 4; ****, p < 0.05 group 2 vs. group 3.Immunohistochemical staining for cells with nuclear deposition of violet pigment were positive(black arrow), nuclear deposition of blue pigment were negative(red arrow) (original magnification 200 ×). Values are means ± SD. Group 1: sham group; Group 2: implantation without ALPPS group; Group 3: implantation/ALPPS group; Group4: implantation/ALPPS/CA group.

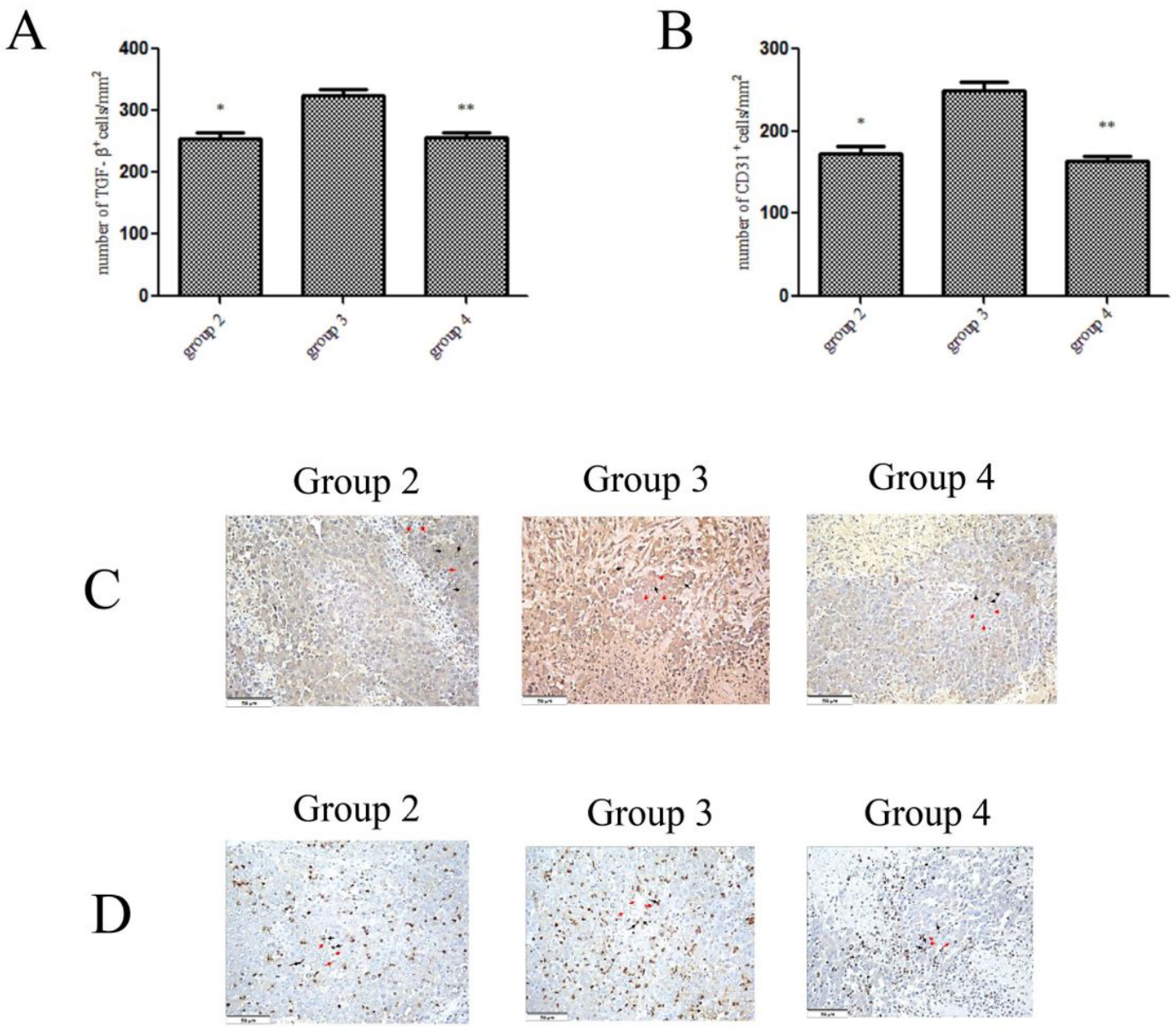

Figure 6

Expression of TGF-β and CD31 in tumors. A, The number of TGF-β+ cells per square millimeter; B, The number of CD31+ cells per square millimeter; C, Immunohistochemical staining for TGF-β+ cells in tumor tissue in each group; D, Immunohistochemical staining for CD31+ cells in tumor tissue in each group. Scale bars, 50μm. *, p < 0.01 group 2 vs. group 3; **, p < 0.01 group 3 vs. group 4; Immunohistochemical staining for cells with nuclear deposition of violet pigment were positive(black arrow), nuclear deposition of blue pigment were negative(red arrow) (original magnification 200 ×). Values are means ± SD. Group 1: sham group; Group 2: implantation without ALPPS group; Group 3: implantation/ALPPS group; Group4: implantation/ALPPS/CA group.

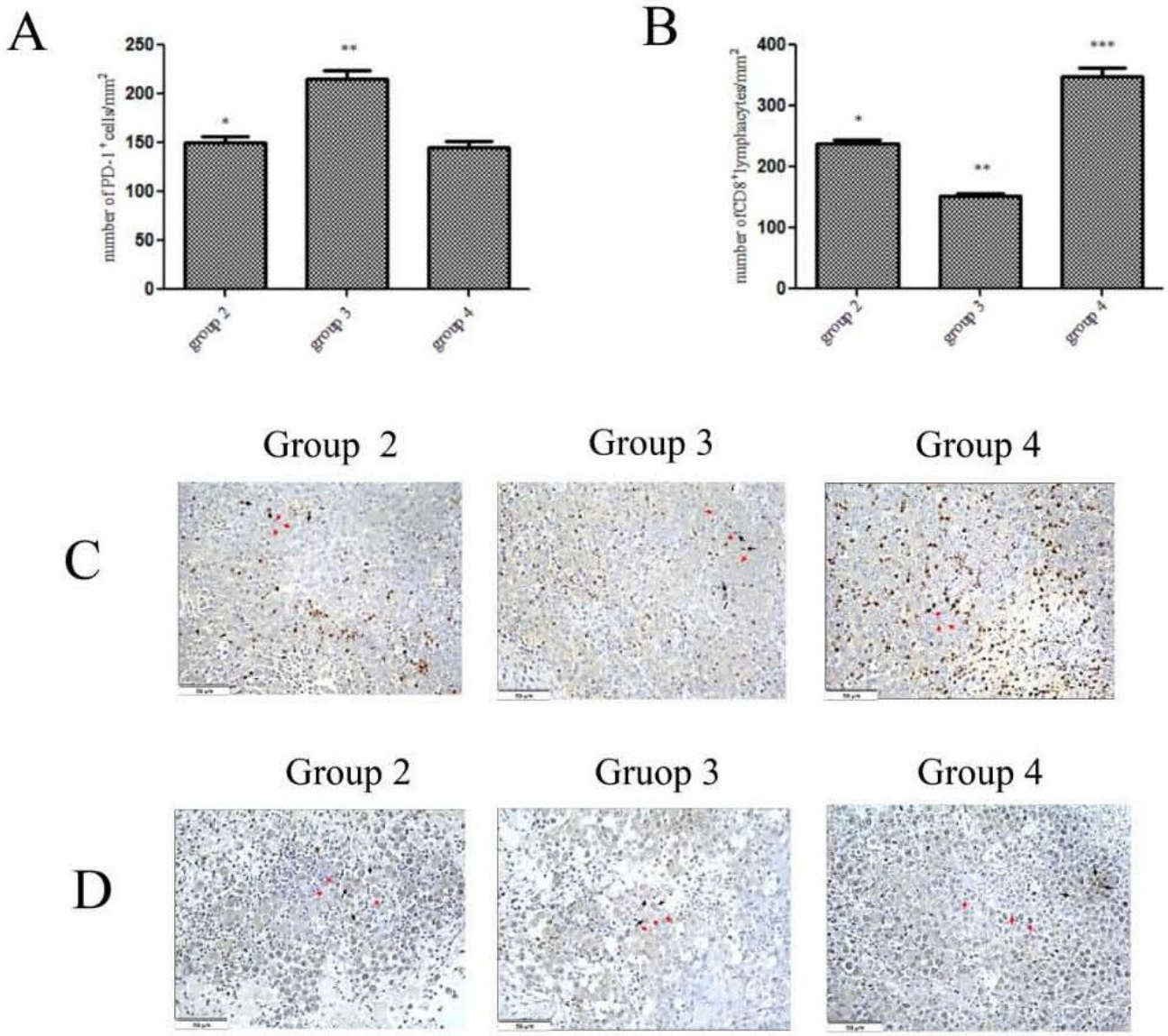

Figure 7

Expression of PD-1 and infiltrated CD8+ lymphocytes in tumors. A, The number of PD-1+ cells per square millimeter; B, The number of CD8+ cells per square millimeter; C, Immunohistochemical staining for PD-

1+ cells in tumor tissue in each group; D, Immunohistochemical staining for CD8+ cells in tumor tissue in each group; E, Immunohistochemical staining negative control image in tumors. Scale bars, 50μm. *, $p < 0.01$ group 2 vs. group 3; **, $p < 0.01$ group 3 vs. group 4; ***, $p < 0.01$ group 2 vs. group 4; Immunohistochemical staining for cells with nuclear deposition of violet pigment were positive(black arrow), nuclear deposition of blue pigment were negative(red arrow) (original magnification 200 ×). Values are means ± SD. Group 1: sham group; Group 2: implantation without ALPPS group; Group 3: implantation/ALPPS group; Group4: implantation/CA group.